Available online at www.sciencedirect.com

ScienceDirect

Advances in Space Research 70 (2022) 2287–2301

ADVANCES IN SPACE RESEARCH (a COSPAR publication)

www.elsevier.com/locate/asr

Multi-objective optimization of low-thrust propulsion systems for multi-target missions using ANNs

Giulia Viavattene *, Enric Grustan-Gutierrez, Matteo Ceriotti

James Watt School of Engineering, University of Glasgow, G12 8QQ Glasgow, United Kingdom

Received 1 February 2022; received in revised form 30 May 2022; accepted 15 July 2022
Available online 22 July 2022

Abstract

Multi-target missions are an attractive solution to visit multiple bodies, increasing the scientific return and reducing the cost, compared to multiple missions to individual targets. Examples of multi-target missions are multiple active debris removals (MADR) and multiple near-Earth asteroids rendezvous (MNR) missions. MADR missions allow for the disposal of inactive satellites, preventing the build-up of space junk, while MNR missions allow to reduce the expenses of each asteroid observation. Since those missions are long and highly demanding in terms of energy, it is paramount to select the most convenient propulsion system so that the propellant mass and the duration of the mission are minimized. To this end, this paper proposes the use of a multi-objective optimization and artificial neural networks. The methodology is assessed by optimizing trajectories for MADR and MNR sequences with off-the-shelf thrusters. Multiple Pareto-optimal solutions can be identified depending on the propulsion system characteristics, enabling mission designers to trade-off the different options quickly and reliably.

Keywords: Low thrust; Artificial neural network; Machine learning; Multi-objective optimization; Space debris removal; Near-earth asteroids

1. Introduction

Interest for multi-target missions is emerging, as they represent an attractive solution to increase the return of a single mission, while reducing the cost with respect to missions with multiple spacecraft to transfer to individual targets (Izzo et al., 2014; Mereta and Izzo, 2018).

Multi-target missions to small objects represent one of the biggest challenges for space engineering (Li et al., 2019). These missions are highly demanding in terms of energy, with a required ΔV which can greatly outrun that of single-object missions. Small satellites can be an attractive solution as they can be propelled by smaller thrusters, reducing the total ΔV of the mission. An additional rationale for smaller satellites is to reduce the cost of launch, since they can be launched as piggyback or from a smaller and cheaper launch vehicle (Aglietti et al., 2020; Wells et al., 2006).

According to the rocket equation, a linear increase in ΔV corresponds to an exponential increase in the propellant mass required to complete the mission (Betts, 1998). For this reason, this study aims at selecting an efficient propulsion system to significantly keep the propellant mass ratio low. Low-thrust technologies, such as electric propulsion (EP), are good candidates because of their high specific impulse (Jahn, 2006; Wertz, 2009).

The use of electric propulsion (EP) for deep-space science missions began with the launch of the Deep Space 1 in 1998. A trade study is performed in Ref. (Brophy, 2003) on advanced propulsion systems for deep-space missions. The study concluded that ion propulsion enables the use of a smaller, less expensive launch vehicle, and significantly shortens the overall trip time. Also, it resulted that

* Corresponding author.
E-mail address: g.viavattene.1@research.gla.ac.uk (G. Viavattene).

https://doi.org/10.1016/j.asr.2022.07.039
0273-1177/

increasing the specific impulse I_{sp} and the maximum power $P_{EP,max}$ (i.e., greater T_{max}) can considerably reduce the required propellant mass. Nevertheless, high values of I_{sp} and $P_{EP,max}$) can result in a sub-optimal system mass (Jahn, 1968). Consequently, a trade-off is necessary to identify the most appropriate propulsion system, depending on the requirements and goals of the missions.

Examples of the multi-target missions, which are currently being investigated and whose demonstrator missions are being designed and flown, are multiple debris removal missions and multiple near-Earth rendezvous missions.

The last two decades have seen the build-up of junk, such as non-functional spacecraft, abandoned launch vehicle stages and other large objects (Bonnal et al., 2013; Liou, 2011; Liou and Johnson, 2008). Removing multiple debris objects in a single active debris removal (MADR) mission (Braun et al., 2013; Berend and Olive, 2013) can be advantageous, beyond the financial prospective. Given the urgency of the clean-up of the overly-crowded low-Earth orbits, MADR missions can have a positive impact from a timing prospective, especially in cases where it is necessary to remove multiple objects within a limited time frame (Van der Pas et al., 2014; Liou, 2011).

The *RemoveDebris* mission was the first mission to successfully demonstrate, in-orbit, a series of technologies that can be used for the active removal of space debris, using a microsat of 100 kg in mass (Aglietti et al., 2020). Astroscale Japan's ADRAS-J, a 80 kg microsatellite with EP capabilities, will launch to rendezvous with debris, demonstrate proximity operations, deliver observational data to better understand the debris environment, and de-orbit debris.[1] Additionally, A. Daykin-Iliopoulos and R. Desai (Daykin-Iliopoulos and Desai, 2014) examined state-of-the-art micro-propulsion options which, thanks to their increased operational capabilities, can be used for demanding missions such as ADR.

Since the 1960s, near-Earth asteroids (NEAs) have also been avidly studied, given the significant role they play in the geological and biological evolution of Earth, the possible exploitation of their resources, and Earth protection from future collisions (Cheng et al., 2017; Lissauer and de Parter, 2013). NEAs vary greatly in size, shape and composition, thus rendezvous and close-up observations are necessary to classify these objects and support any future mitigation action. To reduce the expenses of each observation and increase the possibility of visiting multiple asteroids of interest in a single mission, multiple NEA rendezvous (MNR) missions are preferred (Izzo et al., 2014; Mereta and Izzo, 2018; Peloni et al., 2016; Song and Gong, 2019). Near Earth Asteroid Rendezvous (NEAR) was the first mission flown under NASA's Discovery program with the primary goal to rendezvous with the minor planet 433 Eros (an S-class asteroid) and to gather data on its physical properties.[2] NEOSSat is a Canadian microsatellite mission, with the main purposes of determining and monitoring the NEA orbits that cannot be efficiently detected from the ground, demonstrating the ability of a microsatellite for multi-NEA missions.[3] The novel mission concept called SIMONE (Smallsat Intercept Missions to Objects Near Earth), whereby a fleet of microsatellites may be deployed to individually rendezvous with a number of NEAs at very low cost, assesses the ability to accommodate the necessary electric propulsion, power, payload and other onboard systems within the severe constraints of a microsatellite (Wells et al., 2006).

The design of multi-target missions with low-thrust propulsion requires a complex global optimization problem to be solved, which consists of two coupled sub-problems (Yang et al., 2018). The first is a large combinatorial sub-problem, where the selection of the sequences of objects is performed (Li et al., 2019). The second sub-problem calculates the solution to an optimal control problem (OCP) to identify the optimal flight trajectory with minimum propellant expenditure and/or time of flight (TOF). Since more than 27,000 NEAs are known to date, according to NASA's database,[4] and more than 29,000 space debris objects (for sizes larger than 10 cm) are in Earth orbit, according to a European Space Agency report,[5] the complexity and computational effort involved in solving multi-target problems is exceptional.

Recent studies proposed the use of machine learning, in particular Artificial Neural Networks (ANN), to solve the combinatorial problem and, at the same time, the continuous problem through estimates (Snelling et al., 2021; Viavattene and Ceriotti, 2020a,b). It was demonstrated that a well-trained ANN is able to select high-accuracy solutions, while considerably reducing the computational time. The ANN is integrated within a sequence search algorithm, based on a tree search and breadth-first criterion, which computes the feasible sequences of targets. The candidate sequences which minimize the objective function (e.g., m_{prop} and/or TOF) can be selected and further refined through optimal control problem solvers. Similarly, ANNs have been applied for the fast design of Jovian-moon gravity-assisted transfers (Yan et al., 2022; Yang et al., 2022a) and multiple Jovian-moon three-body flyby missions (Yang et al., 2022b), where ANNs are used to solve the complex restricted three-body-problem dynamics (for which a numerical integration would be otherwise required). In this case, the ANN takes the initial condition of the spacecraft as inputs and calculates the final conditions of the gravity-assisted transfer or at flyby, respec-

[1] astroscale.com/astroscale-selects-rocket-lab-to-launch-phase-i-of-jaxas-debris-removal-demonstration-project, accessed on 2021-10-17.

[2] solarsystem.nasa.gov/missions/near-shoemaker/in-depth/, accessed on 2021-11-07.

[3] earth.esa.int/web/eoportal/satellite-missions/n/neossat, accessed on 2021-11-07.

[4] cneos.jpl.nasa.gov/orbits/elements.html, accessed on 2021-10-17.

[5] www.esa.int/Safety_Security/Clean_Space/How_many_space_debris_objects_are_currently_in_orbit, accessed on 2021-10-17.

tively, as outputs. An ANN was also employed in the determination of multiple NEA missions using solar sails with a characteristic acceleration $a_c = 0.75$ mm/s^2 (Song and Gong, 2019). Similarly, ANNs are used to find a solution to other multi-target optimization problems, such as multiple time-optimal (or fuel-optimal) low-thrust transfers and J_2-perturbed multi-impulse transfers (Li et al., 2019).

From the analysis of the previous studies (Li et al., 2019; Snelling et al., 2021; Song and Gong, 2019; Viavattene and Ceriotti, 2020a,b), it can be noted that the ANNs are trained with a fixed low-thrust propulsion system, which is selected a priori. Therefore, the ANN requires retraining every time that the use of thrusters with other characteristics is explored, since these will affect the cost and duration of the transfers. This process may be particularly time-consuming, especially in the mission design phase, during which the identification of the optimal low-thrust propulsion system to fly the mission generally involves several iterations to identify the most suitable propulsion system among a range of propulsion capabilities. This study aims to show that an ANN can both identify the most convenient trajectories for the sequence of objects for MADR and MNR missions, and consider different options of low-thrust propulsion systems so that the most adequate one for these missions can be selected. This would enable the design of an ANN which can be used for different mission scenarios and different propulsion capabilities, without the need to be retrained when the thruster characteristics change. From the literature review, it can be noticed that the use of ANNs to scan through multiple low-thrust options for multi-target missions remains largely unexplored, and the approach proposed in this paper aims to fill this gap, in aid of future mission designers.

Two objective functions are considered when optimizing the EP system: the total duration of the mission and the initial mass of the system (which includes the mass of the propulsion system and the propellant mass). A propulsion system which minimizes the duration of the mission does not necessarily optimize the initial spacecraft mass. In fact, no unique solution exists that simultaneously minimizes both objectives. These objectives are conflicting criteria. This represents a multi-objective non-linear optimization problem, for which a set of mathematically equally good solutions can be identified, which are known as Pareto-optimal solutions (Branke et al., 2008; Miettinen, 1999). To solve such a problem, the ANN is combined with a multi-objective genetic algorithm (GA).

In summary, this study analyzes the effects of different characteristics of a propulsion system on multi-target missions. Ultimately, the proposed methodology of an ANN and multi-objective optimization can provide a method for a fast optimization of the propulsion system so that the objectives of a given mission can be achieved, in terms of duration or initial mass required. An ANN is trained to quickly estimate the cost of a trajectory in terms of m_{prop} and TOF, given the debris orbits and propulsive characteristics. The proposed methodology can identify candidate sequences of objects which, flown with the optimized propulsion system, minimize the objective functions according to the mission goals. The selected sequences can be further refined through optimal control problem solvers.

The paper is organized as follows. A description of the proposed methodology which uses the multi-objective GA and the ANN (GA-ANN) is provided in Section 2. Section 3 describes the dynamics of the multi-target missions. The ANN is designed in Section 4, where the generation of the training database is also discussed and the performance of the network is analyzed. In Section 5, optimal MADR and MNR sequences are analyzed and the performance of the proposed methodology is assessed. Finally, Section 6 provides a summary of the methodology and the findings.

2. Multi-objective optimization

Current low-thrust thrusters offer a range of characteristics and capabilities to propel at different values of specific impulse I_{sp} and maximum thrust T_{max}.[6] An accurate selection of the appropriate propulsion system can lead to missions with shorter time of flight and less propellant mass required. This is paramount for multi-target missions which are highly demanding in terms of energy.

In an effort to study how the choice of the propulsion system can affect the performance of multi-target missions and to ultimately identify the optimal propulsion system for any given mission, the optimization logic which is schematically presented in Fig. 1 has been developed. Two nested optimizations are performed: (i) the inner optimization to find the minimum initial mass m_0 (for a fixed payload mass) and (ii) the outer optimization over I_{sp} and T_{max} of the EP system, to minimize the two objective functions, i.e. the initial mass, m_0, and the TOF, $t_{0,f}$.

The outer optimization is solved by a multi-objective GA. The objective is to analyze how the selection of the propulsion capabilities affects the mission in terms of cost (i.e., required initial mass m_0 which, as will be specified below, depends on the propellant mass and EP-system mass) and duration. As both m_0 and TOF are objective functions of the GA, a multi-objective optimization (also known as Pareto optimization) is conducted. The multi-objective optimization entails the process of multiple-criteria decision making, which is applied in cases where optimal decisions need to be taken in the presence of trade-offs between two or more conflicting objectives (Branke et al., 2008).

The multi-objective GA identifies a number of Pareto-optimal solutions, all of which are considered equally good. The optimal solutions are obtained for different values of I_{sp} and T_{max} and the selection of one solution over the

[6] www.enpulsion.com/order/, accessed on 2021-11-10.

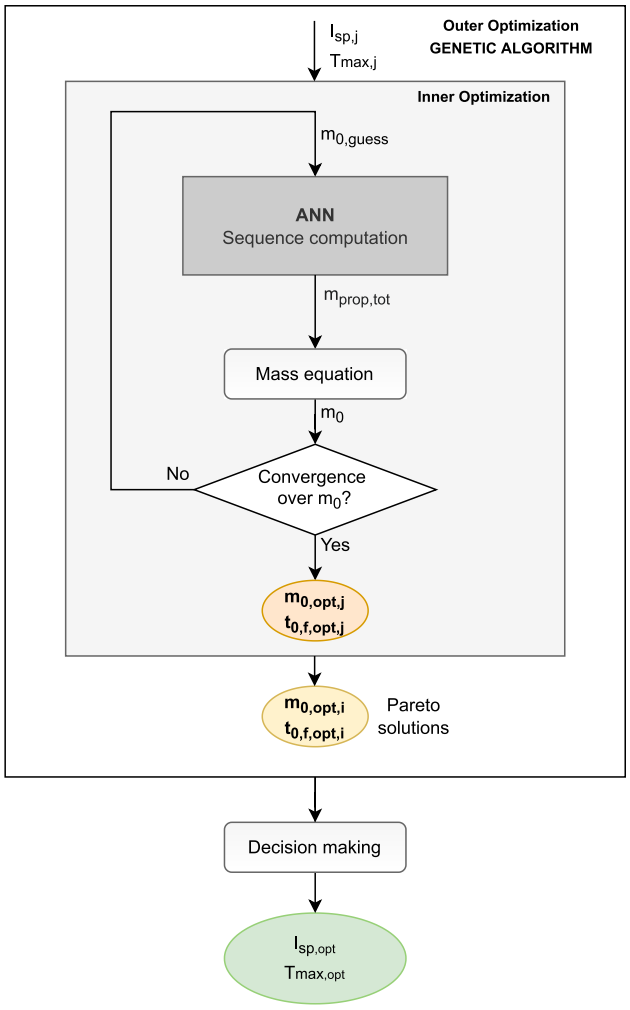

Fig. 1. Diagram of the optimization logic.

others depends on the goals and/or requirements of the mission.

For each combination of $I_{sp,j}$ and $T_{max,j}$, with $j = (1, \ldots, N_p)$ and N_p given by the product of the number of generations times the population size in a generation, the evaluation of the objective functions requires the multi-objective GA to run the inner optimization, and estimate the optimal $m_{0,opt,j}$ and duration $t_{0f,opt,j}$, which can be obtained with the given EP system. To this end, the ANN is trained, as discussed in Section 4, and used to compute the cost of low-thrust transfers, given the orbital parameters of the initial and final object, the characteristics of the propulsion system (i.e., I_{sp} and T_{max}), and the mass of the spacecraft at the beginning of the transfer. In particular, the ANN estimates the total propellant mass and TOF required to fly the full sequence of objects with the given propulsion system and initial mass.

The objective of the inner optimization is to identify the minimum initial mass which allows to fly the given multi-target mission when an EP system with $I_{sp,j}$ and $T_{max,j}$ is used. Once the propellant mass is calculated by the ANN for a preliminary mass budget, the total spacecraft mass m_0 can be calculated as (Ceriotti and McInnes, 2011):

$$m_0 = m_{prop} + m_{tank} + n_{thrusters}(m_{EP} + m_{gimbal}) + m_{pl} \quad (1)$$

where each component can be described as follows:

- m_{prop} is the propellant mass necessary to fly the desired mission with duration equal to the TOF estimated by the ANN
- m_{tank} is the mass of the tanks and can be expressed as a function of the propellant mass (Gershman and Seybold, 1999):

$$m_{tank} = 0.1 m_{prop} \quad (2)$$

- $n_{thrusters}$ is the number of thrusters of the propulsion system.
- m_{EP} is the mass of a thruster, which is a function of its power and, at a first approximation, can be expressed as:

$$m_{EP} = k_{EP} P_{EP,max} \quad (3)$$

with k_{EP} is an empirical constant (Jahn, 1968) and $P_{EP,max}$ being the maximum power required by the thruster, which is a function of the maximum thrust available during the mission and of the specific impulse:

$$P_{EP,max} = \frac{T_{max} I_{sp} g_0}{2\eta_{EP}} \quad (4)$$

where $\eta_{EP} = 0.7$ is the efficiency of the propulsion system to convert electrical energy (Kitamura et al., 2007). In this work, off-the-shelf thrusters are considered, so the mass of the individual thruster m_{EP} is fixed to the mass of the thruster selected, as specified in Section 3.3.

- m_{gimbal} is the mass of EP gimbal system which is included when more than one thruster are used, with the purpose of compensating the misalignment of the thrust vector produced by the thrusters with respect to the center of mass of the spacecraft. The gimbal mass needs to be proportional to the mass of the thrusters:

$$m_{gimbal} = \rho_{gimbal} m_{EP} \quad (5)$$

with $\rho_{gimbal} = 0.1$.

- m_{pl} is the payload mass, which in this case includes the structure and masses of all the required systems a part from the propulsion system and the propellant mass.

Substituting the above expressions, Eq. (1) can be written as follows:

$$m_0 = (1 + 0.1) m_{prop} + n_{thrusters}(1 + 0.1) m_{EP} + m_{pl} \quad (6)$$

where it can be concluded that minimizing the initial mass m_0 corresponds to optimizing the propellant mass m_{prop} and the number of thrusters $n_{thrusters}$, given that m_{EP} and m_{pl} are fixed.

The propellant mass, which is calculated by the ANN, is a function of the initial mass m_0, the ΔV required to perform the transfer, and the specific impulse of the propulsion system I_{sp}, as defined by the rocket equation (Betts, 1998):

$$m_{\text{prop}} = m_0\left(1 - e^{\frac{\Delta V}{I_{\text{sp}} g_0}}\right) \tag{7}$$

with $\mathbf{g}_0$ being the gravitational acceleration at the Earth's surface.

In the proposed inner optimization procedure, also illustrated in Fig. 1, a guessed initial mass $m_{0,\text{guess}}$ is used as input to the ANN, which calculates the total cost and duration of the given multi-target mission. From the ANN output, which provides an estimation of m_{prop}, and from the values of $I_{\text{sp},j}$ and $T_{\text{max},j}$, which allow to identify the number of thrusters needed, the initial mass m_0 can be recalculated using Eq. (6). The resulting value of m_0 is compared to the guessed initial mass $m_{0,\text{guess}}$ and, if the absolute value of the difference $|m_0 - m_{0,\text{guess}}| \leqslant \epsilon$ with $\epsilon = 10^{-5}$, convergence is reached and the minimum initial mass $m_{0,\text{opt},j}$ to fly the desired mission is identified. Otherwise, the process is repeated using m_0 as the updated guessed initial mass, i.e. $m_{0,\text{guess}} = m_0$. This procedure is performed iteratively, until convergence. Once the inner optimization converges, the TOF is calculated by the ANN and set as the optimal TOF, $t_{0,\text{f,opt,j}}$, which is required to fly the mission with this minimum initial mass $m_{0,\text{opt},j}$ and the given propulsion system ($I_{\text{sp},j}$ and $T_{\text{max},j}$).

In conclusion, the multi-objective optimization process, GA-ANN, where the multi-objective GA and the trained ANN are used in the outer and inner optimizations, computes the Pareto optimal solutions which are the output solution vectors of the objective functions $\mathbf{y}_{\text{GA,opt,i}}$ at the values $\mathbf{x}_{\text{GA,opt,i}}$ of the input variables of the multi-objective GA, with:

$$\mathbf{x}_{\text{GA,opt,i}} = [I_{\text{sp,i}}, T_{\text{max,i}}] \tag{8}$$

$$\mathbf{y}_{\text{GA,opt,i}} = [m_{0,\text{opt,i}}, t_{0,\text{f,opt,i}}] \tag{9}$$

where i indicates the i-th Pareto solution with $i = (1, \ldots, N_{\text{GA}})$ and N_{GA} being the total number of Pareto solutions identified by the GA. A final optimal solution with $\mathbf{x}_{\text{GA-ANN}} = [I_{\text{sp,opt}}, T_{\text{max,opt}}]$ and $\mathbf{y}_{\text{GA-ANN}} = [m_{0,\text{opt}}, t_{0,\text{f,opt}}]$can be selected among the Pareto-optimal solutions following a decision making process, so that the goals and requirements of the mission can be met.

3. Dynamics of the system

In this section, the dynamics of the multi-target missions is presented, where the spacecraft is modeled as a point mass with continuous low-thrust. The dynamics of the system can be described using the following differential equation (Betts, 2010):

$$\dot{\mathbf{x}}(t) = \mathbf{A}(\mathbf{x})\mathbf{a} + \mathbf{b}(\mathbf{x}) \tag{10}$$

where $\mathbf{x}$ is the state vector of modified equinoctial elements, $\mathbf{x} = [p, f, g, h, k, L]$ (Betts, 1998); $\mathbf{a}$is the perturbing acceleration in radial, transversal, and out-of-plane components; $\mathbf{A}(\mathbf{x})$ and $\mathbf{b}(\mathbf{x})$ are the matrix and the vector of the dynamics, respectively. A full definition of $\mathbf{A}(\mathbf{x})$ and $\mathbf{b}(\mathbf{x})$ can be found in Ref. (Betts, 2010).

For the MADR missions, the perturbing acceleration, $\mathbf{a}$, is given by (i) the acceleration due to the thrust $\mathbf{a_T}$ (acting only on the chaser and not on the debris objects), (ii) the acceleration due to the oblateness of the Earth $\mathbf{a_g}$ and (iii) the acceleration due to atmospheric drag $\mathbf{a_D}$. Differently, for MNR missions, the effects of the Earth's oblateness and atmosphere are negligible and only propulsion disturbances are considered, i.e.:

$$\text{for MADRs}: \quad \mathbf{a} = \mathbf{a_T} + \mathbf{a_g} + \mathbf{a_D} \tag{11}$$

$$\text{for MNRs}: \quad \mathbf{a} = \mathbf{a_T} \tag{12}$$

The acceleration of the spacecraft due to the thrust $\mathbf{a_T}$ is formulated as:

$$\mathbf{a_T} = \frac{T_{\text{max}}}{m}\mathbf{N} \tag{13}$$

where T_{max} is the maximum thrust of the propulsion system, m is the mass of the system and $\mathbf{N} = [N_r, N_\theta, N_h]^T$ indicates the acceleration direction and magnitude vector in radial, transverse, and out-of-plane coordinates. The mass of the system m decreases with time due to the propellant consumption as described by the following mass differential equation:

$$\dot{m} = -\frac{T_{\text{max}}|\mathbf{N}|}{I_{\text{sp}} g_0} \tag{14}$$

For MADRs the gravitational acceleration, due to the Earth's oblateness and generally mass density distribution, is experienced by both the chaser and debris objects, as well as the acceleration due to the atmospheric drag.

The gravitational acceleration is experienced by both the chaser and debris objects in MADR missions, due to the Earth's oblateness and mass density distribution in the north-south direction (i.e. zonal harmonics only). It can be defined as follows (Wakker, 2015):

$$\mathbf{a_g} = \mathbf{Q_r^T}\delta\mathbf{g} \tag{15}$$

where $\mathbf{Q_r} = [\mathbf{i_r}, \mathbf{i}_\theta, \mathbf{i_h}]$ is the transformation matrix from the rotating local-vertical-local-horizontal (LVLH) frame to the Earth-centered inertial (ECI) frame and $\delta\mathbf{g}$ is the gravitational perturbation acceleration. The full definition of $\mathbf{Q_r}$ and $\delta\mathbf{g}$ can be found in Ref. (Viavattene et al., 2022).

The acceleration due to the atmospheric drag in the radial, transverse and normal components can be defined as (Wakker, 2015):

$$\mathbf{a_D} = [a_{D_r} \; a_{D_\theta} \; 0] \tag{16}$$

where the out-of-plane component of $\mathbf{a_D}$ is negligible, as the net plane change is close to zero. The radial and transverse components are defined as follows:

$$a_{D_r} = -0.5\rho S C_D v v_r \tag{17}$$

$$a_{D_\theta} = -0.5\rho S C_D v v_\theta \tag{18}$$

where ρ is the atmospheric density, which can be estimated using the Exponential Atmospheric Model, which considers the atmosphere as composed by an ideal gas at constant

temperature in a hydrostatic equilibrium (Schroeder, 2000). This model is a compromise between accuracy and ease of implementation and considered appropriate for the level of the study. Also, S is the aerodynamic surface area, C_D is the drag coefficient and v is the velocity magnitude, i.e. $v = \sqrt{v_r^2 + V_\theta^2}$, with v_r and v_θ being its radial and tangential components (Wakker, 2015).

3.1. Multiple active debris removals

A MADR mission requires the chaser to rendezvous and dock with the first debris object in the sequence and descent to a disposal low-Earth orbit. The object is released for de-orbiting and re-entry before the chaser transfers to the next target object. The procedure repeats until the propellant mass is depleted. Fig. 2 provides a representation of the mission scenario, where Di with $i = [1, 2, \ldots]$ indicates the debris object located at different altitudes and $\Delta\Omega$ is the difference in right ascension of the ascending node (RAAN) between debris orbits.

In this case study of MADR, some assumptions are considered to keep the model simple and, consequently, minimize the computational time required to generate the database to train the ANN. Although these assumptions are chosen to be representative of a real MADR mission, they could be easily varied for future use-cases simply by re-training the ANN with the desired model.

A set of debris objects on circular orbits at the same inclination is considered. This is a reasonable assumption because the current satellite constellations are often on circular orbits, at the same inclination and spaced in RAAN. To perform the rendezvous transfers from a space debris object to the other, the chaser has to match the altitude and right ascension of the ascending node Ω (RAAN) of the orbit of the arrival body (Debris 2, or D2) at the arrival epoch, while departing from the departure body (Debris 1, or D1). Since the spiral low-thrust transfer legs between debris exhibits a large number of revolutions, the phasing along the orbit between the chaser and debris can be neglected as it can be attained with minimal propulsion effort.

To minimize the propellant consumption, it is chosen to use the thrust to obtain the change in altitude and to exploit the Earth's oblateness gravitational perturbation (J_2) to achieve the change in Ω through RAAN-phasing orbits. The orbital-averaged RAAN variation rate is given by the Gauss equations as follows (Curtis, 2005):

$$\dot{\Omega} = -\left[\frac{3}{2}\frac{J_2\sqrt{\mu}R^2}{a^{7/2}(1-e^2)^2}\cos(i)\right] \tag{19}$$

which is experienced by both the chaser and the debris objects. The optimal altitude where to perform the RAAN-phasing can be selected so that the propellant mass and/or TOF are minimized (Viavattene et al., 2022).

3.2. Multiple NEA rendezvous

During an MNR mission the spacecraft is expected to rendezvous multiple NEAs, i.e., matching the position and velocity of the asteroid so that proximity operations can be conducted. Fig. 3 provides a schematic representation of the mission scenario, where Ai with $i = [1, 2, \ldots]$ indicates the NEA object located on different orbits. Compared to the MADR case, a level of complexity is added for MNR missions where also objects with inclined and eccentric orbits are considered. Consequently, it will be possible to test the GA-ANN performance when a more complex system dynamics is considered.

Determining the cost and duration of a low-thrust transfer, given the departure and arrival NEA orbital characteristics, requires a low-thrust optimal control problem to be solved. This is very computationally expensive and requires an accurate first guess to identify an appropriate solution (Alemany and Braun, 2007). To reduce the computational time and effort, different methodologies have been developed to avoid the full low-thrust optimization and identify an approximated solution. The shape-based approach is used in this study. The shape of the minimum-cost rendezvous transfer is defined analytically and can be approx-

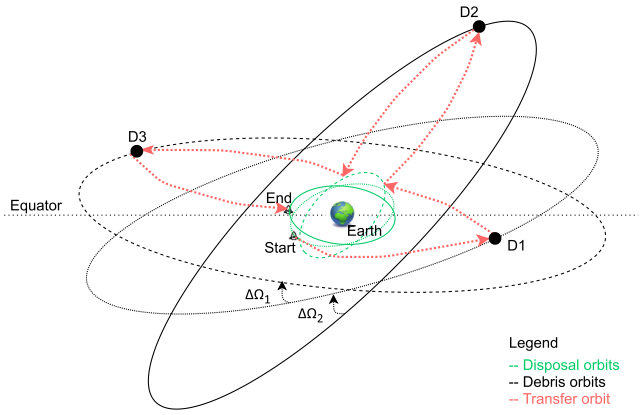

Fig. 2. Schematic representation of the MADR mission scenario.

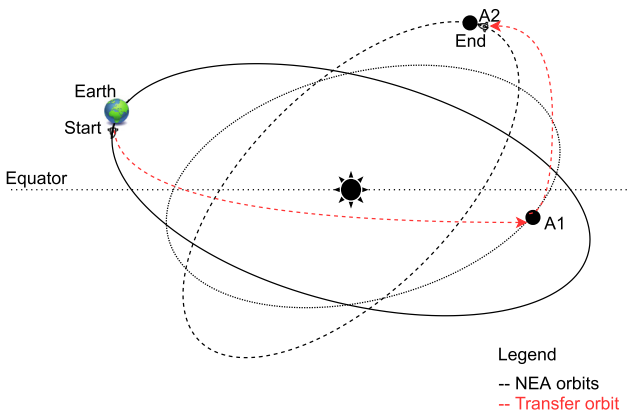

Fig. 3. Schematic representation of the MNR mission scenario.

imated for the given range of launch dates with zero departure and arrival velocity, TOF, and the number of revolutions (Taheri and Abdelkhalik, 2012; Li et al., 2014; De Pascale and Vasile, 2006). Thus, this choice is appropriate for the preliminary search to design MNRs.

According to the shape-based method, a transfer $\mathbf{r}(t)$ is defined as a parametrized analytical curve connecting two points in a central force field (Petropoulos and Longuski, 2000; De Pascale and Vasile, 2006):

$$\mathbf{x} = \mathbf{x_0} + \mathbf{x_1}(L - L_0) + \boldsymbol{\lambda}\sin(L - L_0 + \phi) \tag{20}$$

which defines the solution of the full 3-D transfer based on a set of modified equinoctial elements $\mathbf{x} = [p, f, g, h, k, L]^T$. The vector $\boldsymbol{\lambda} = [\lambda_1, \lambda_2, \lambda_3]$ has as components the shaping parameters, which are determined using a genetic algorithm; $\mathbf{x}_0$ and $\mathbf{x}_1$ are defined from the boundary conditions; and the phase parameter ϕ is empirically set.

The acceleration which the propulsion system has to provide to fly the calculated transfer is obtained by computing the control thrust required to satisfy the dynamics, as follows:

$$\mathbf{a} = \ddot{\mathbf{r}} + \mu\frac{\mathbf{r}}{r^3} \tag{21}$$

where μ is the gravitational parameter of the central body (in this case, the Sun) and $\mathbf{r}$ is the position vector in the Cartesian reference frame.

For each individual transfer between two selected bodies, the shape-based method is used to compute the propellant mass and duration required to fly the transfer. The training database is built by storing, for each transfer, the parametrization of the orbits of the departure and arrival asteroids, the angular position of the asteroids at the departure date, and the cost and TOF of the minimum-mass transfer.

3.3. Low-thrust propulsion systems

The choice of the on-board propulsion system to perform high-ΔV missions, such as multiple-target missions, has a major impact on the cost (in terms of mass required and, consequently, launch cost) and duration. As mentioned, low-thrust systems can be beneficial for this type of missions because it allows to deliver the same ΔV using less propellant than high-thrust systems (Wertz, 2009).

Instead of considering the propellant mass alone, the number of thrusters (which defines the total mass of the EP system) is also included in the optimization of this study. As mentioned, off-the-shelf thrusters are used in this application, thus the mass of the individual thruster is considered fixed. The time of flight of the transfers is also an essential parameter which needs to be taken into consideration for a complete analysis on the feasibility of EP systems for multi-target missions. The reason for this is to investigate how the choice of the propulsion system affects the design of a multi-target mission.

In fact, a mission could be flown with an EP system with certain values of I_{sp} and T_{max} which allow to reduce the propellant mass, at cost of a higher m_{EP}, which may have a negative impact on the launch cost, and higher TOF, which translates into the mission being completed at a later stage. The opposite case can also happen. Considering the full initial mass m_0 and TOF in the optimization and trade study offers space mission designers the possibility to choose the most appropriate propulsion system on the basis of their mission requirements and objectives.

In this work, EP systems for small satellites are considered, but the same analysis and considerations could be expanded to larger satellites or different types of propulsion systems. One crucial challenge to enhance the flexibility and allow multi-target missions with such small spacecraft is to develop a small, lightweight, compact and efficient EP system. Many thrusters are available on the market, with different characteristics. The models of the thrusters by Enpulsion®. are selected as they offer a wide range of thrust and specific impulse.

For the MADR mission, the Micro R3 thruster is selected, with the operational envelope being presented in Fig. 4(a). The operational envelope is obtained by approximating the ranges of maximum thrust which can be obtain for certain values of specific impulse, according to the capability of the thruster, as detailed in the product specifications.[7] For a fixed I_{sp}, any increase in T_{max} results in a higher operational power (which might result in higher external power systems mass). It should be noted that, the values of I_{sp} and T_{max} which are considered as input to the multi-objective GA are values corresponding to an operational point inside the operational envelope of the EP system. Also, although the Micro thruster is offered with a fixed amount of propellant mass, this is neglected at this stage since the minimum amount of propellant mass to fly the mission, as calculated by the ANN, is considered and subject to the optimization as part of the total initial mass m_0. Also, the lifetime constraints of the thrusters is not considered at this stage of the analysis, but it can be easily implemented if additional thrusters (which equates to an additional mass) are used to compensate for degradation.

It is noted that the Micro R3 is a scaled technology of the Enpulsion Nano thruster.[8] Similarly, as the MNR missions generally require greater propulsion capabilities than the MADR, the capabilities of the Micro R3 thrusters are scaled up to obtain a thruster, referred in this paper as Mini thruster, which can thrust with greater T_{max} than the Micro R3. This is achieved, to a first approximation, by simply scaling up the T_{max} achievable of the Micro R3 by a factor of 4, resulting in an operational envelope of the Mini thruster which is shown in Fig. 4(b).

[7] www.enpulsion.com/wp-content/uploads/ENP2018-002.H-MICRO-Thruster-Product-Overview.pdf, accessed on 2021-11-21.
[8] www.enpulsion.com/order/, accessed on 2021-11-21.

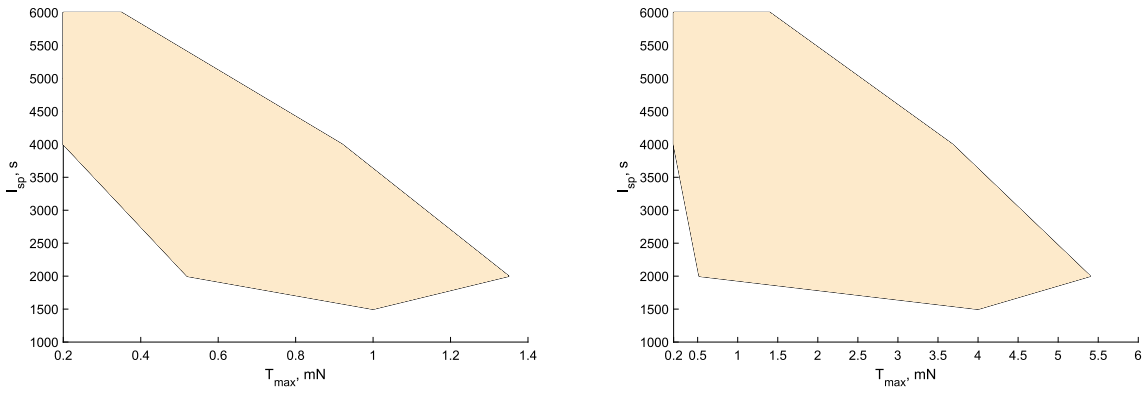

(a) Micro R3 thruster (b) Mini thruster

Fig. 4. Propulsive capabilities of the selected thrusters.[8]

These off-the-shelf thrusters are engineered in a modular approach, with units clustering easily together to form building blocks that can be arranged for various mission profiles. The mass of one thruster is $m_{\mathrm{EP,MicroR3}} = 2.6$ kg and $m_{\mathrm{EP,Mini}} = 9.8$ kg for the Micro R3 and Mini thruster, respectively. Considering that the individual thruster mass is fixed (i.e., m_{EP} is fixed in Eq. (1)), the parameter that varies in the multi-objective optimization is, apart from the propellant mass, the number of thrusters.

The motivation for employing more than one thruster is that the thruster operational envelope (Figs. 4(a) and 4(b)) stretches towards greater maximum values of $T_{\max}$. For this study, the maximum number of thrusters allowed is 15.

4. ANN for multi-target missions

An ANN is trained to approximate the system dynamics described in Section 3 so that, given the orbital elements of the departure body B_1, arrival body B_2 and propulsion system (inputs), the ANN can provide a quick estimation of the propellant mass and TOF (outputs) required to transfer from B_1 to B_2, i.e.:

$$\mathbf{y} = [m_{\mathrm{prop}}, t_{0,f}] \tag{22}$$

The training database contains the inputs and the desired outputs (targets), which are used during the training of the network. In particular, considering the differences in the dynamics and assumptions between the MADR and MNR missions, the *input vector* $\mathbf{x}$ can be defined:

- for MADR:

$$\mathbf{x} = [h_{\mathrm{D1}}, \Omega_{\mathrm{D1}}, m_{\mathrm{D1}}, h_{\mathrm{D2}}, \Omega_{\mathrm{D2}}, m_{\mathrm{SC}}, I_{\mathrm{sp}}, T_{\max}] \tag{23}$$

  where h and Ω are the altitude and RAAN of the departure ($D1$) and arrival ($D2$) debris; m_{D1} is the mass of the departure debris, which needs to be carried to disposal; m_{SC} is the initial mass of the chaser, which varies during the mission due to the propellant consumption; I_{sp} and $T_{\max}$ describe the propulsion system characteristics.
- for MNR:

$$\mathbf{x} = [\mathbf{x}_{\mathrm{MEE,A1}}, \mathbf{x}_{\mathrm{MEE,A2}}, m_{\mathrm{SC}}, I_{\mathrm{sp}}, T_{\max}] \tag{24}$$

  where $\mathbf{x}_{\mathrm{MEE}}$ are the modified equinoctial elements of departure ($A1$) and arrival ($A2$) asteroid; m_{SC} is the initial spacecraft mass, varying during the mission due to the propellant consumption; I_{sp} and $T_{\max}$ describe the propulsion properties.

A multi-layered feedforward ANN is selected for this case study, as it is demonstrated to approximate any non-linear mapping $\mathbf{y}_t = \mathbf{f}(\mathbf{x})$ to any degree of accuracy (Goodfellow et al., 2016). In order for the network to approximate the desired function (*network function*) appropriately, the network needs to be trained with a database containing the corresponding inputs and desired outputs (or targets). The training of the network is achieved by optimizing the weights and biases associated to each neuron to minimize the network loss function, i.e., the mean squared error $\mathscr{E}_{\mathrm{MSE}}$ between the outputs generated by the network $\mathbf{y}$ and the targets $\mathbf{y}_t$:

$$\mathscr{E}_{\mathrm{MSE}} = \frac{1}{N}\sum_{i=1}^{N}||\mathbf{y}_i - \mathbf{y}_{t,i}||^2 \tag{25}$$

with N being the number of outputs.

The training database for the MADR case is generated by randomly selected 150,000 pairs of fictitious debris objects, with altitudes between 500 and 1500 km and mass between 100 and 300 kg. The inclination is fixed to 87.9 deg and the disposal orbit is at an altitude of 390 km. The chaser mass can vary from 40 kg to 140 kg.

Similarly, for the MNR case, 50,000 pairs of NEAs[9] are randomly selected to define the training database of the ANN. Asteroids with eccentricity below 0.4 and inclination below 20 deg are used, as the highly inclined and highly eccentric objects would require a larger cost and duration to transfer to and from. The mass of the spacecraft can vary from 40 kg to 220 kg. In the MNR case, a larger range

[9] Data available through the link https://ssd.jpl.nasa.gov/sbdb_query.cgi#x (accessed on 2021-11-01).

is allowed for the initial mass because a higher thrust (thus, a heavier propulsion system) and a greater propellant mass is generally required for this kind of mission compared to the MADR missions.

The effect of changing the values of the network hyper-parameters and architecture on the final performance are analyzed so that the values which allow to achieve a higher performance can be selected (Viavattene and Ceriotti, 2020a). Two networks (one for the MADR case and one for the MNR case) with four hidden layers and 80 neurons using the sigmoid as activation function are built. The pre-processing steps performed are the batch normalization of the training data. To detect and prevent overfitting, the training databases are divided into 70% training set, 15% validation set and 15% test set (Kurková, 1992). The former is used to train the network. Following the training, the validation set is used to eventually evidence the presence of overfitting during the training and the test set is used to evaluate the final performance of the network. Levenberg-Marquardt is used as a training algorithm, with an initial value of the gradient constant μ of 0.001 and a decrease factor of 0.1.

4.1. Performance analysis

As the validation set includes samples which are not used for the training, the validation-set MSE is often used as a performance indicator. Additionally, regression plots and the related correlation coefficients are used to illustrate how well the network outputs (Y-axis) fit the targets (X-axis) with respect to the training, validation, test sets and overall. A perfect fit of the outputs and targets is obtained when the data fall along the line with a unit slope and zero y-intercept, i.e., $y = x$ and correlation coefficient $R = 1$.

Figs. 5 and 6 show the performance of the trained network for MADR and MNR, respectively. In both figures, the plot (a) presents the regression analysis of the network outputs and the targets for the train, validation and test sets. The final overall correlation coefficient is 0.99 for MADR and 0.97 for MNR, which indicates that the ANN is able to approximate the fitness function which relates inputs and outputs for both types of multi-target missions.

The performance plot (b) shows how for each training epoch the MSE decreases until the performance goal is met (such as in the MADR case, Fig. 5(b) or before the training starts overfitting (such as in the MNR case, Fig. 6(b)). The latter case is verified when the validation-set MSE becomes to increase while the training-set MSE continues to decrease. The final validation-set MSE of 0.022 for the MADR case and 0.191 for the MNR case suggests a very accurate performance of the trained networks. These values of MSE correspond to a mean error of propellant mass and TOF of, respectively, 0.3% and 2.1% (for MADR) and 1.5% and 2.9% (for MNR), which are calculated between the output y_i and the target $y_{t,i}$ as:

$$\mathscr{E}_y = \frac{1}{N}\sum_{i=1}^{N}\frac{y_i - y_{t,i}}{y_{t,i}} \cdot 100 \tag{26}$$

where y can be either the propellant mass or TOF.

The ANN trained for the MADR missions achieves a better performance than the ANN for the MNR missions, as it can be noticed from both the regression and performance plots. This can be linked to the increased complexity of the MNR model compared to the MADR model, which are detailed in Section 3. In particular, the change of inclination and eccentricity from an orbit to the next one; and

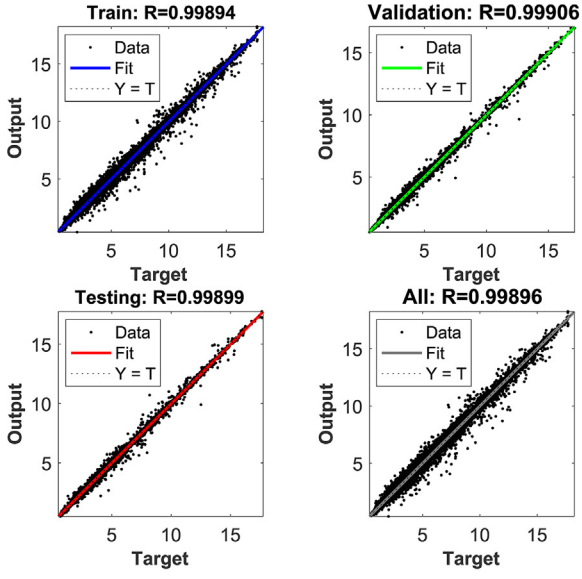

(a) Regression

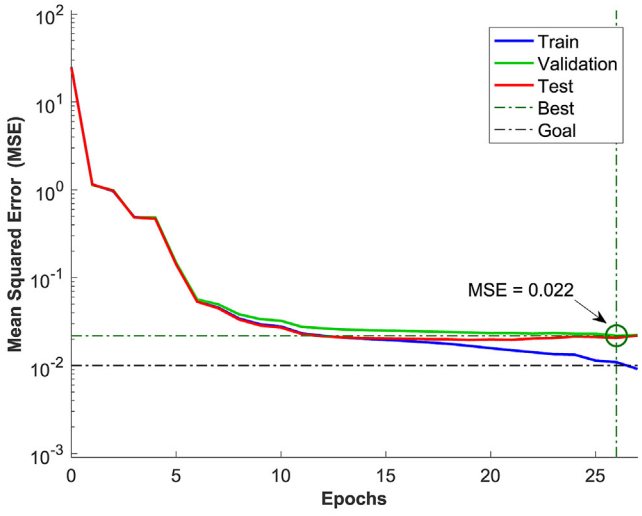

(b) Performance

Fig. 5. Regression (a) and performance (b) analysis of the ANN trained for MADR missions.

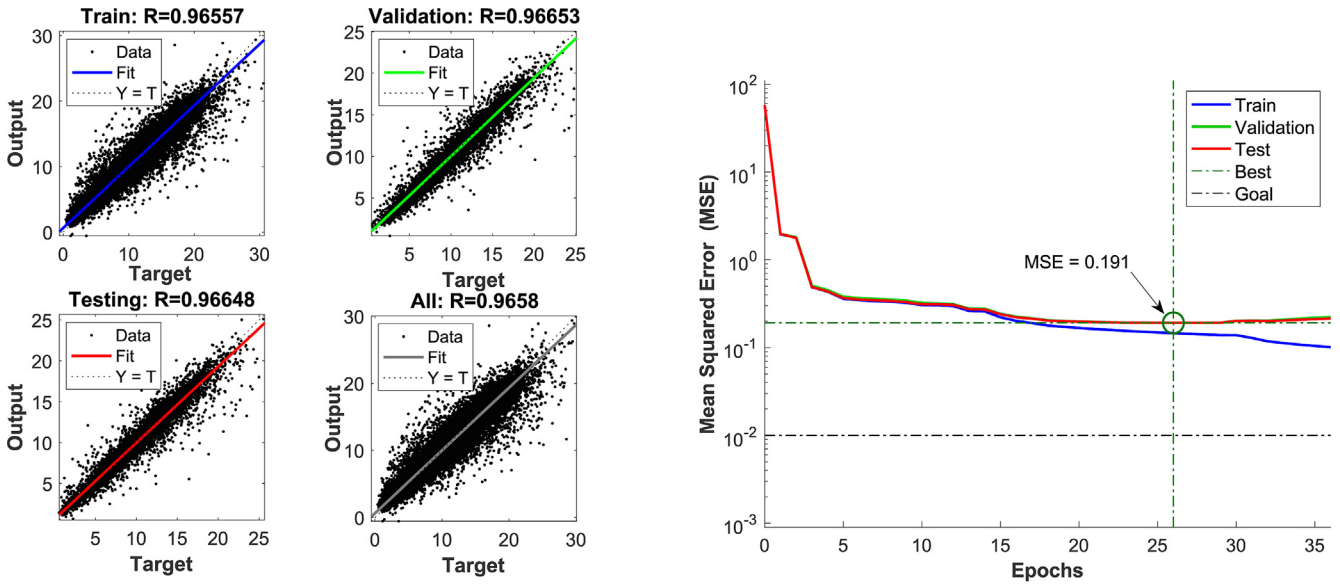

(a) Regression (b) Performance

Fig. 6. Regression (a) and performance (b) analysis of the ANN trained for MNR missions.

the use of the GA in the shape-based model to find the cost and duration for the optimal transfer, in MNR case. Also, it can be noticed that for MADR the training is complete when the performance goal is reached in the training set (blue line), while for the MNR case, the training is complete because of the early stopping method which is used to avoid overfitting (i.e., the training is stopped when the validation-set MSE starts increasing, while the training-set MSE continues to decrease).

The impact of the use of ANNs on the computational time for the estimation of the cost and duration of multi-target missions is assessed by comparing the performance with current methods employed in the industry. For MADR, the current method consists of an industry expert processing the same input and providing the best solution possible within 4 h via an iterative approach (Snelling et al., 2021). For MNR, the proposed methodologies suggest to use a simplified model to identify the sequences of asteroids and, successively, convert these solutions into feasible low-thrust trajectories by means of an optimization. For instance, in the method used by Peloni et al. (Peloni et al., 2016), the shape-based method is used as the simplified model.

For the comparison, the same set of input data and the same assumptions are used. For MADR, the computational time required by ANN is more than 26 times faster than the time required by the methods employed by the industry (Snelling et al., 2021). This result was obtained with only 100 debris objects in the database, and it is expected that the benefits of using the SS-ANN method become even more important when a larger set of satellites is considered. A detailed description of the analysis can be found in (Viavattene et al., 2022).

For MNR, when the same input data (2,768 objects) and assumptions are considered, the use of the ANN makes the algorithm almost 100 times faster compared to the method in Ref. (Peloni et al., 2016), while maintaining a comparable level of accuracy. This is because as the number of sequences or objects to analyze increases, the number of permutations to calculate increases exponentially; thus, the advantages of using an ANN and the difference in computational time will be greater. Please refer to Ref. (Viavattene and Ceriotti, 2021) for the complete analysis on computational speed.

5. Multi-target missions

The optimal MADR and MNR sequences, identified in Refs. (Viavattene et al., 2022 and Viavattene and Ceriotti, 2021), respectively, are used to demonstrate the capabilities of the proposed methodology. These sequences were selected in the referenced works using a sequence search (SS) algorithm. The logic of the algorithm is based on a tree-search method and breadth-first criterion. Each node of the tree represents a transfer leg and how one proceeds through its branches depends on the mission objectives which, in this case, is the TOF minimization. The SS works by selecting a body B_j as departure object and B_i as arrival object, with j and $i \in [1, N]$ so that all the possible permutations between the N objects in the database can be evaluated. The trained ANN is used to calculate the m_{prop} and TOF of each low-thrust transfer. At this point, the arrival object becomes the departure object of the following leg and the same procedure is iterated. The sequence is complete once the total mission duration exceeds 10 years (or until the depletion of the propellant mass).

For larger number of objects, the complexity and required memory of the tree search grow factorially. The motion of each object along its orbit needs to be calculated and updated at each iteration. Therefore, each node of the search tree is designed to record the orbital parameters of the selected target at the departure time, current flight time, current propellant mass expenditure, and the quality of the transfer to reach the selected target (i.e., m_{prop} and $t_{0,f}$, as calculated by the ANN).

In the following sections, the performance of the proposed methodology, in which a multi-objective optimization is used in combination with the trained ANNs, is demonstrated in term of the accuracy to identify the most convenient low-thrust capabilities to fly multi-target missions by optimizing the thrusting properties on the basis of the mission objectives, i.e., desired duration of the whole mission and initial launch mass, as described in Section 2.

5.1. MADR mission design

The selected MADR sequence from Ref. (Viavattene et al., 2022) (Table 3, Sequence B) allows for the disposal of 11 debris objects in 10.87 years with a required propellant mass of 60.76 kg, when the initial mass is 400 kg. In this study, a trajectory through the same sequence will be optimized for using a micro-satellite equipped with the Micro R3 low-thrust thrusters.

Fig. 7 illustrates the Pareto front obtained from the multi-objective GA and the trained ANN. Plot (a) shows the values of I_{sp} and T_{max} associated to the optimal points in the Pareto plot (b), which presents the two objective functions, namely the TOF and $m_{0,opt}$. The colors of points in the plots depend on the number of thrusters on-board to achieve the desired T_{max}, going from 1 (deep blue) to 15 (dark red), as indicated in the color bar.

The computational time required to run the multi-objective GA and ANN is 42.48 min. Considering that the GA is recomputing the sequence multiple times with different values and combinations of I_{sp} and T_{max}, it can be appreciated how the use of the ANN allows to considerably reduce the computational time, as discussed in Section 4.1.

It can be noticed that, with highest values of I_{sp} and lowest values of T_{max} (minimum number of thrusters), solutions with minimum $m_{0,opt}$ are obtained, at the expenses of the TOF which is exponentially high. Differently, lowest values of I_{sp} and highest values of T_{max} (larger number of thrusters) allow for solutions with minimum TOF, at the expenses of an higher initial mass. This tool offers the mission designer the opportunity to investigate each option and select the point along the Pareto front which better suits the mission objectives.

In this case we selected a point just after the elbow in the Pareto front (indicated by the arrow in the plots of Fig. 7), where an initial mass of 72.04 kg (of which 11.05 kg are propellant mass) and total TOF 9.13 years are achieved when using seven Micro R3 thrusters which deliver a $I_{sp} = 3265$ s and $T_{max} = 7.30$ mN. This sequence is recalculated by solving the dynamics of the system to obtain the exact values of mass and transfers' duration. Also, these values can be used for a comparison with the ANN values and evaluate the accuracy of the ANN.

Table 1 presents the characteristics (altitude h, RAAN, and mass m) of the objects de-orbited as part of the optimized MADR sequence and the mission characteristics (propellant mass m_{prop} and TOF). Additionally, Fig. 8 illustrates the altitude and used propellant mass of the spacecraft along the sequence. The final duration of the mission is 9.02 years and it requires a propellant mass of 11.86 kg (achieving a propellant mass ratio $m_{prop}/m_0 = 0.16$). It follows that the GA-ANN methodology is able to identify the TOF and propellant mass of the system with an error of approximately 1.2% and 6.8%, respectively. Additionally, this shows the advantages of using a micro-satellite to fly MADR missions. In fact, when comparing these results with those obtained in Ref. (Viavattene et al., 2022), the same sequence requires about 60.76 kg of propellant mass, when the initial mass is 400 kg

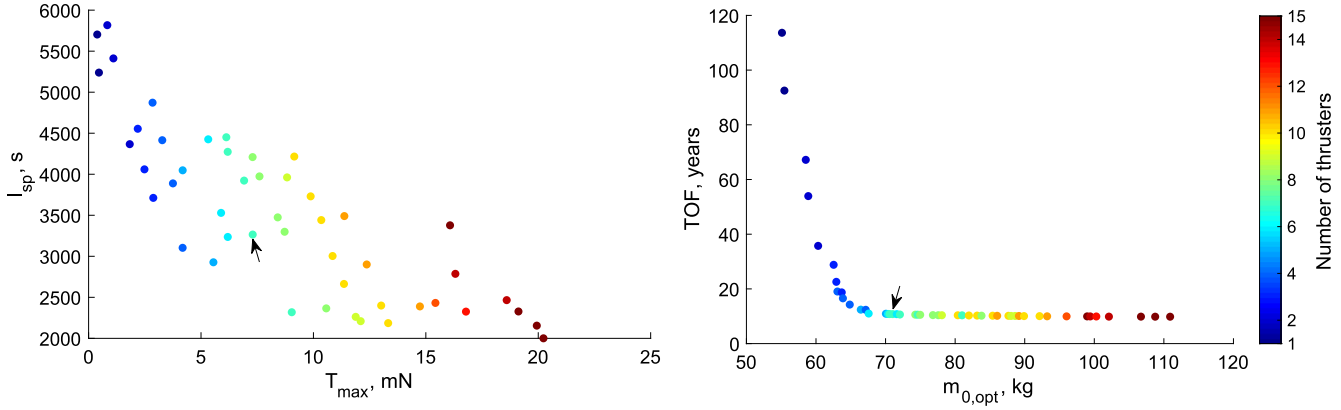

(a) I_{sp} and T_{max} (b) Pareto front

Fig. 7. Low-thrust propulsion characteristics (a) and Pareto front (b) for the MADR mission.

Table 1
Characteristics of the selected MADR sequence.

Debris	h, km	RAAN, deg	m, kg	TOF, days	m_{prop}, kg
D1	661.73	162.03	131.24	N/A	N/A
D2	504.96	158.72	270.37	295	1.14
D3	577.40	149.33	163.74	254	0.95
D4	534.05	145.48	256.27	405	2.02
D5	517.24	145.16	253.91	195	0.99
D6	514.14	138.62	139.19	426	0.95
D7	534.61	128.19	213.67	282	0.67
D8	667.95	84.76	222.82	213	1.05
D9	694.88	66.66	200.81	313	1.74
D10	517.45	123.32	171.80	431	1.59
D11	588.01	88.94	213.15	178	0.76

for $m_{prop}/m_0 = 0.15$. It follows that a comparable propellant mass ratio is achieved, however using a microsatellite allows to reduce the initial mass (and, consequently, the propellant mass and launch mass), for a comparable duration of the mission.

5.2. MNR mission design

To study the performance of GA-ANN for the MNR case, a sequence which was obtained in Ref. (Viavattene and Ceriotti, 2021) (Tables 8 and 9, Sequence C) is selected. This sequence allowed to visit six asteroids in less than 10 years, requiring a total ΔV of 17.95 km/s for an initial launch mass of 1000 kg, $I_{sp} = 3000$ s and $T_{max} = 0.1$ N.

Apart from identifying the most appropriate propulsion system which optimizes the TOF and m_0 of the basis of the mission objectives, this analysis aims to prove how such a mission could be flown by a small satellite to reduce the launch mass costs.

Fig. 9 illustrates the Pareto front obtained from the GA-ANN methodology. Plot (a) shows the values of I_{sp} and T_{max} associated to the optimal points in the Pareto plot (b), which presents the two objective functions, namely the TOF and $m_{0,opt}$. The colors of the points in the plots depend on the number of thrusters on-board to achieve the desired T_{max}, going from 1 (deep blue) to 15 (dark red), as indicated in the color bar.

Similarly to the MADR mission, high values of I_{sp} and small value of T_{max} allow to fly the sequence with minimum initial mass but in a considerably longer amount of time. On the other hand, relatively low values of I_{sp} and high value of T_{max} allow to fly the sequence faster but a higher initial mass is required. It should be noticed that, differently from the MADR case where all the I_{sp} values were considered to provide an optimal solution within the Pareto front, for MNR only values of I_{sp} larger than 3500 s give a solution in the Pareto front. This means that values below 3500 s of specific impulse result in a mission associated with larger TOF and/or larger initial mass.

The point in the Pareto front (indicated by the arrow in the plots of Fig. 9), which is selected for further optimization, corresponds to an initial mass of 120.10 kg (of which 43.42 kg are propellant mass) and total TOF 11.91 years and a propulsion system with $I_{sp} = 4082$ s and $T_{max} = 10.81$ mN. This sequence is recalculated by solving the dynamics of the system and finding the optimal solution. The optimal control problem is solved by using a discrete non-linear programming (NLP) together with a variable-order adaptive Radau collocation method (Patterson and Rao, 2014; Rao et al., 2010; Garg et al., 2011), encoded in IPOPT (Wachter and Biegler, 2006).

Table 2 presents the characteristics of the transfers, namely departure and arrival dates, TOF, m_{prop} and stay time at the asteroid to allow for proximity operations. Additionally, Fig. 10 illustrates the heliocentric ecliptic-plane view of the complete trajectory.

It results that a small satellite of 120.10 kg is able to fly the NEA sequence equipped with three Mini low-thrust thrusters. The total duration of the mission is 11.44 years and requires 42.40 kg of propellant mass (achieving a

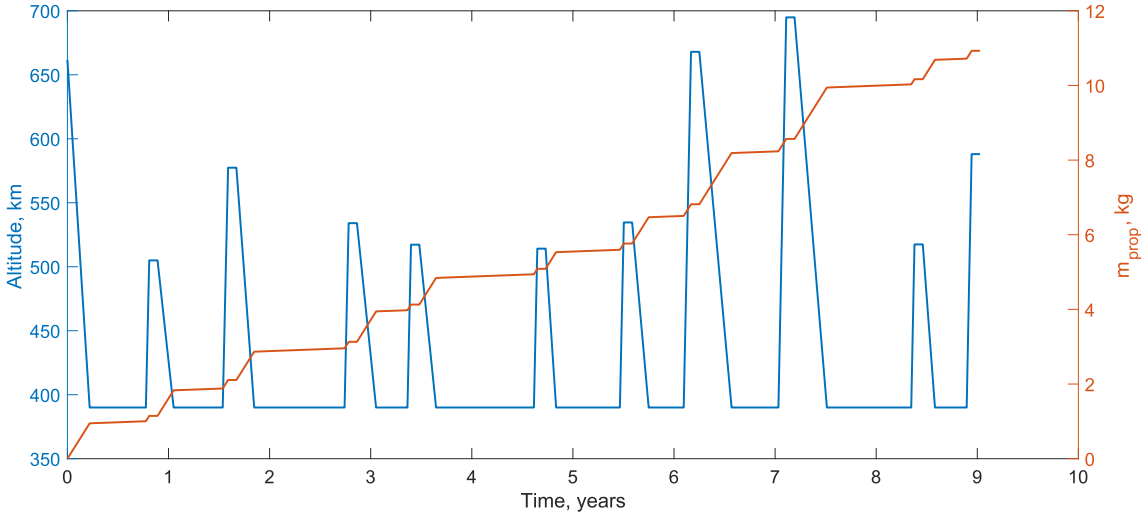

Fig. 8. Altitude and propellant mass for the MADR sequence.

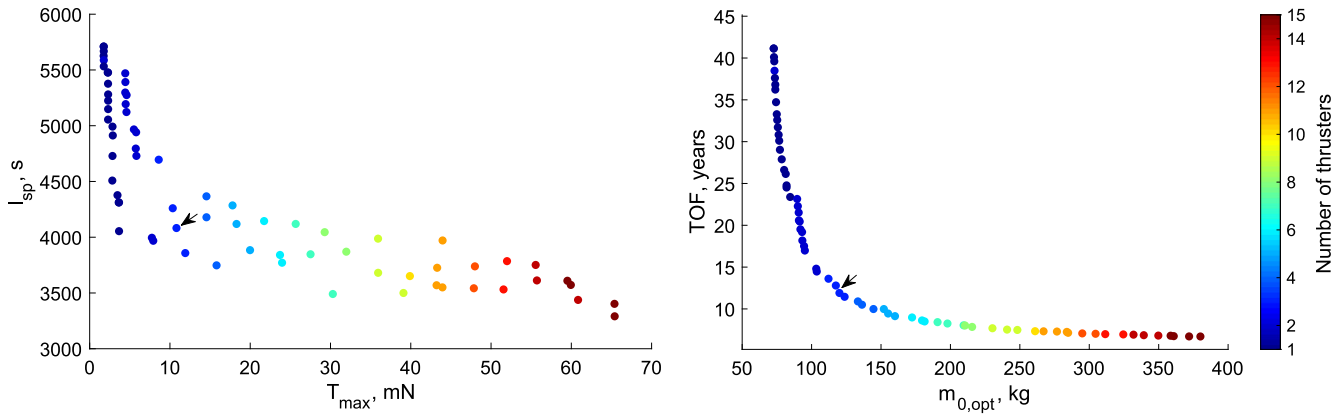

(a) I_{sp} and T_{max} (b) Pareto front

Fig. 9. Low-thrust propulsion characteristics (a) and Pareto front (b) for the MNR mission.

Table 2
Characteristics of the selected MNR sequence.

Leg	Departure	Arrival	TOF, days	m_{prop}, kg	Stay Time, days
Earth - 2014 WX202	2035-03-12	2036-11-25	625	6.01	50
2014 WX202 - 2008 EA9	2037-01-17	2038-12-24	706	5.70	86
2008 EA9 - 2015 VO142	2039-03-21	2040-03-19	364	5.03	180
2015 VO142 - 2012 EP10	2040-09-15	2041-04-01	197	4.45	50
2012 EP10 - 2013 CY	2041-05-21	2043-11-21	913	9.89	50
2013 CY - 2014 UV210	2044-01-10	2046-08-24	956	11.32	–

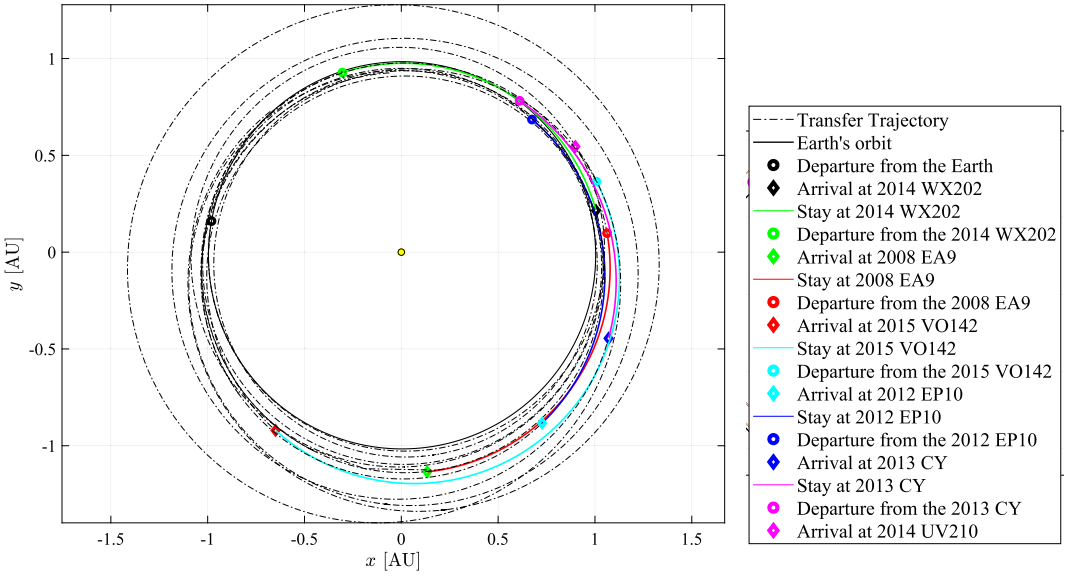

Fig. 10. MNR sequence: heliocentric ecliptic-plane view.

propellant mass ratio $m_{prop}/m_0 = 0.35$). Comparing the optimized results with those obtained by the ANN, it follows that a percentage error of 4.1% for the TOF and 2.4% for the total propellant mass is obtained.

Finally, the same sequence was optimized with a system of initial mass 1500 kg and requiring around 685 kg of propellant mass so that $m_{prop}/m_0 = 0.46$ (Viavattene and Ceriotti, 2021). In this case, the use of a small satellite allows to reduce the propellant mass ratio. This analysis demonstrated that a small satellite equipped with the appropriate low-thrust EP system is able to fly the same sequence in a similar amount of time. As a consequence of using a small satellite, the necessary propellant mass and initial launch mass can be significantly reduced.

6. Conclusions

The proposed methodology (GA-ANN) uses a multi-objective genetic algorithm (GA) optimization in combination with an artificial neural network (ANN) to identify the most convenient low-thrust system to fly multi-target missions. Multiple active debris removal (MADR) missions and multiple NEA rendezvous (MNR) missions are considered as case studies.

The logic of the optimization which has been developed includes an inner optimization over the initial mass m_0, where the ANN is used to estimate the cost and duration of each transfer, and an outer optimization performed by the GA over the propulsion properties, namely specific impulse I_{sp} and maximum thrust T_{max}. This allows to investigate the effects of different propulsion capabilities on multi-target missions in terms of the cost (i.e., m_0) and duration. Pareto-optimal solutions are identified for different values of I_{sp} and T_{max}.

The GA-ANN methodology is assessed with MADR and MNR sequences. In both cases, a point along the Pareto front is selected for further analysis and optimization. The error in mission duration and cost between the values computed by GA-ANN and the optimal values is on average lower than 3% and 5%, respectively.

It can be concluded that the proposed methodology is able to identify Pareto-optimal solutions for different low-thrust capabilities, so that mission designers can quickly analyze the options available and select the solution which most suits the objectives and requirements of the mission. The use of miniaturized electric thrusters can enable, when technologically feasible, small satellites to fly multi-target missions, providing advantages in terms of reduced propellant mass and initial launch mass, while completing the mission in comparable amounts of time.

Declaration of Competing Interest

The authors declare that they have no known competing financial interests or personal relationships that could have appeared to influence the work reported in this paper.

Acknowledgments

Giulia Viavattene gratefully acknowledges the support received for this research from the James Watt School of Engineering at the University of Glasgow for funding the research under the James Watt sponsorship program.

References

Aglietti, G., Taylor, B., Fellowes, S., Ainley, S., Tye, D., Cox, C., Zarkesh, A., Mafficini, A., N., V., Bashford, K., Salmon, T., Retat, I., Burgess, C., Hall, A., Chabot, T., Kanani, K., Pisseloup, A., Bernal, C., Chaumette, F., Pollini, A., Steyn, W.H., 2020. RemoveDEBRIS: An in-orbit demonstration of technologies for the removal of space debris. Aeronaut. J. 124 (1271), 1–23. https://doi.org/10.1017/aer.2019.136.

Alemany, K., Braun, R.D., 2007. Survey of Global Optimization Methods for Low- Thrust, Multiple Asteroid Tour Missions. In: 17th AAS/AIAA Space Flight Mechanics Meeting, AAS 07-211, pp. 1–20.

Berend, N., Olive, X., 2013. Bi-objective optimization of a multiple-target active debris removal mission. Acta Astronaut. 122.

Betts, J.T., 1998. Survey of Numerical Methods for Trajectory Optimization. J. Guidance Control Dyn. 21(2), 193–207. doi: https://doi.org/10.2514/2.4231. URL: http://arc.aiaa.org/doi/10.2514/2.4231.

Betts, J.T., 2010. Practical Methods for Optimal Control and Estimation Using Nonlinear Programming, second ed. SIAM Press, Philadelphia.

Bonnal, C., Ruault, J., Desjean, M., 2013. Active debris removal: recent progress and current trends. Acta Astronautica. Acta Astronaut., 85

Branke, J., Deb, K., Miettinen, K., Slowinski, R., 2008. Multiobjective Optimization. Springer, Heidelberg.

Braun, V., Lupken, A., Flegel, S., Gelhaus, J., Mockel, M., Kebschull, C., Wiedemann, C., Vörsmann, P., 2013. Active debris removal of multiple priority targets. Adv. Space Res. 51 (9).

Brophy, J., 2003. Advanced Ion Propulsion Systems for Affordable Deep-Space Missions. Acta Astronaut. 52 (2–6), 309–316. https://doi.org/10.1016/S0094-5765(02)00170-4.

Ceriotti, M., McInnes, C., 2011. Systems design of a hybrid sail pole-sitter. Adv. Space Res. 48 (11), 1754–1762. https://doi.org/10.1016/j.asr.2011.02.010.

Cheng, B., Yu, Y., Baoyin, H., 2017. Asteroid surface impact sampling: dependence of the cavity morphology and collected mass on projectile shape. Adv. Space Res. 7 (10004).

Curtis, H., 2005. Orbital Mechanics for Engineering Students. Elsevier.

Daykin-Iliopoulos, A., Desai, R., 2014. Performance evaluation of micropropulsion systems with the application of Active Debris Removal. In: 50th AIAA/ASME/SAE/ASEE Joint Propulsion Conference, vol. 3540. https://doi.org/10.2514/6.2014-3540.

De Pascale, P., Vasile, M., 2006. Preliminary Design of Low-Thrust Multiple Gravity-Assist Trajectories. AIAA J. Spacecraft Rockets 43 (5), 1065–1076. https://doi.org/10.2514/1.19646.

Garg, D., Patterson, M.A., Francolin, C., Darby, C.L., Huntington, G.T., Hager, W.W., Rao, A.V., 2011. Direct trajectory optimization and costate estimation of finite-horizon and infinite-horizon optimal control problems using a Radau pseudospectral method. Comput. Optimiz. Appl. 49 (2), 335–358. https://doi.org/10.1007/s10589-009-9291-0.

Gershman, R., Seybold, C., 1999. Propulsion trades for space science missions. Acta Astronaut. 45 (4–9), 541–548.

Goodfellow, I., Bengio, Y., Courville, A., 2016. Deep Learning. The MIT Press, Cambridge, Massachusetts.

Izzo, D., Simoes, L.F., Yam, C.H., Biscani, F., Di Lorenzo, D., Bernardetta, A., Cassioli, A., 2014. GTOC5: Results from the European Space Agency and University of Florence. Acta Futura 8 (November), 45–56. https://doi.org/10.2420/AF08.2014.45.

Jahn, R.G., 1968. Physics of Electric Propulsion. McGraw-Hill, New York, 2–10.

Jahn, R.G., 2006. Physics of Electric Propulsion. McGraw-Hill Book Company, New York.

Kitamura, S., Ohkawa, Y., Hayakawa, Y., Yoshida, H., Miyazaki, K., 2007. Overview and Research Status of the JAXA 150-mN Ion Engine. Acta Astronaut. 61 (1–6), 360–366. https://doi.org/10.1016/j.actaastro.2007.01.010.

Kurková, V., 1992. Kolmogorov's theorem and multilayer neural networks. Neural Netw. 5 (3), 501–506. https://doi.org/10.1016/0893-6080(92)90012-8.

Li, S., Zhu, Y., Wang, Y., 2014. Rapid Design and Optimization of Low-Thrust Rendezvous/Interception Trajectory for Asteroid Deflection Missions. Adv. Space Res. 53 (4), 696–707.

Li, H., Chen, S., Izzo, D., Baoyin, H., 2019. Deep Networks as Approximators of Optimal Transfers Solutions in Multitarget Missions. Acta Astronaut. https://doi.org/10.1016/j.actaastro.2019.09.023.

Liou, J., 2011. A parametric study on using active debris removal for LEO environment remediation. Adv. Space Res. 47 (11).

Liou, J., Johnson, N.L., 2008. Instability of the present LEO satellite populations. Adv. Space Res. 41 (7), 1046–1053.

Lissauer, J.J., de Parter, I., 2013. Fundamental Plantary Science. Cambridge University Press.

Mereta, A., Izzo, D., 2018. Target selection for a small low-thrust mission to near-Earth asteroids. Astrodynamics 2(3), 249–263. arXiv: arXiv:1802.02418v1.

Miettinen, K., 1999. Nonlinear Multiobjective Optimization. Kluwer Academic Publishers.

Van der Pas, N., Lousada, J., Terhes, C., Bernabeu, M., Bauer, W., 2014. Target selection and comparison of mission design for space debris removal by DLR's advanced study group. Acta Astronaut. 102.

Patterson, M.A., Rao, A.V., 2014. GPOPS-II: A MATLAB Software for Solving Multiple-Phase Optimal Control Problems usign hp-Adaptive Gaussian Quadrature Collocation Methods and Sparse Nonlinear Programming. ACM Trans. Math. Softw. 41 (1). https://doi.org/10.1145/2558904.

Peloni, A., Ceriotti, M., Dachwald, B., 2016. Solar-Sail Trajectory Design for a Multiple Near-Earth-Asteroid Rendezvous Mission. J. Guid. Control Dyn. 39 (12), 2712–2724. https://doi.org/10.2514/1.G000470.

Petropoulos, A.E., Longuski, J.M., 2000. Automated Design of Low-Thrust Gravity-Assist Trajectories. AIAA Paper, 2000–4033.

Rao, A.V., Benson, D.A., Darby, C.L., Patterson, M.A., Francolin, C., Sanders, I., Huntington, G.T., 2010. Algorithm 902: GPOPS, a MATLAB Software for Solving Multiple-Phase Optimal Control Problems using the Gauss Pseudospectral Method. ACM Trans. Math. Softw. 37 (2). https://doi.org/10.1145/1731022.1731032. arXiv:1005.3014.

Schroeder, D.V., 2000. An Introduction to Thermal Physics, 3rd ed. Addison-Wesley.

Snelling, D., Devereux, E., Payne, N., Nuckley, M., Viavattene, G., Ceriotti, M., Wokes, S., Di Mauro, G., Brettle, H., 2021. Innovation in Planning Space Debris Removal Missions Using Artificial Intelligence and Quantum-Inspired Computing. In: 8th European Conference on Space Debris, Darmstadt, Germany, 20-23 Apr.

Song, Y., Gong, S., 2019. Solar-Sail Trajectory Design of Multiple Near Earth Asteroids Exploration Based on Deep Neural Network. Aerosp. Sci. Technol. 91, 28–40. https://doi.org/10.1016/j.ast.2019.04.056.

Taheri, E., Abdelkhalik, O., 2012. Shape Based Approximation of Constrained Low-Thrust Space Trajectories using Fourier Series. J. Spacecraft Rockets 49 (3), 535–546.

Viavattene, G., Ceriotti, M., 2020a. Artificial neural network design for tours of multiple asteroids. Springer, Lectures Notes in Computer Science,. https://doi.org/10.1007/978-3-030-61705-9_63.

Viavattene, G., Ceriotti, M., 2020b. Low-thrust multiple asteroid missions with return to Earth using artificial neural networks. In: AAS/AIAA Astrodynamics Specialist Conference.

Viavattene, G., Ceriotti, M., 2021. Artificial Neural Networks for Multiple NEA Rendezvous Missions with Continuous Thrust. AIAA J. Spacecraft Rockets. https://doi.org/10.2514/1.A34799.

Viavattene, G., Devereux, E., Snelling, D., Payne, N., Wokes, S., Ceriotti, M., 2022. Design of multiple space debris removal missions using machine learning. Acta Astronaut. 193, 277–289. https://doi.org/10.1016/j.actaastro.2021.12.051.

Wachter, A., Biegler, L.T., 2006. On the Implementation of an Interior-Point Filter Line-search Algorithm for Large-scale Non-linear Programming. Math. Program. 106 (1), 25–57. https://doi.org/10.1007/s10107-004-0559-y.

Wakker, K.F., 2015. Fundamentals Of Astodynamics. Faculty of Aerospace Engineering, Delft University of Technology.

Wells, N., Walker, R., Green, S., Ball, A., 2006. SIMONE: Interplanetary Microsatellites for NEO Rendezvous Missions. Acta Astronaut. 59, 700–709. https://doi.org/10.1016/j.actaastro.2005.07.036.

Wertz, J.R., 2009. Orbit & Constellation Design & Management. Springer, New York.

Yan, J., Yang, H., Li, S., 2022. ANN-based method for fast optimization of Jovian-moon gravity-assisted trajectories in CR3BP. Adv. Space Res. 69 (7), 2865–2882. https://doi.org/10.1016/j.asr.2022.01.019.

Yang, B., Feng, J., Huang, X., Li, S., 2022a. Hybrid method for accurate multi-gravity-assist trajectory design using pseudostate theory and deep neural networks. Sci. China Technol. Sci. 65, 595–610. https://doi.org/10.1007/s11431-021-1933-7.

Yang, H., Yan, J., Li, S., 2022b. Fast computation of the Jovian-moon three-body flyby map based on artificial neural networks. Acta Astronaut. 193, 710–720. https://doi.org/10.1016/j.actaastro.2021.08.054.

Yang, H., Tang, G., Jiang, F., 2018. Optimization of observing sequence based on nominal trajectories of symmetric observing configuration. Astrodynamics 2 (1), 25–37. https://doi.org/10.1007/S42064-017-0009-2.